Surface-Guided Core-Shell ZnSe@ZnTe Nanowires as Radial p-n Heterojunctions with Photovoltaic Behavior

Article

Surface-Guided Core-Shell ZnSe@ZnTe Nanowires as Radial p-n Heterojunctions with Photovoltaic Behavior

Eitan Oksenberg, Sara Martí-Sànchez, Ronit Popovitz-Biro, Jordi Arbiol, and Ernesto Joselevich

ACS Nano, **Just Accepted Manuscript** • Publication Date (Web): 15 May 2017

Published article available at: http://dx.doi.org/10.1021/acsnano.7b02199

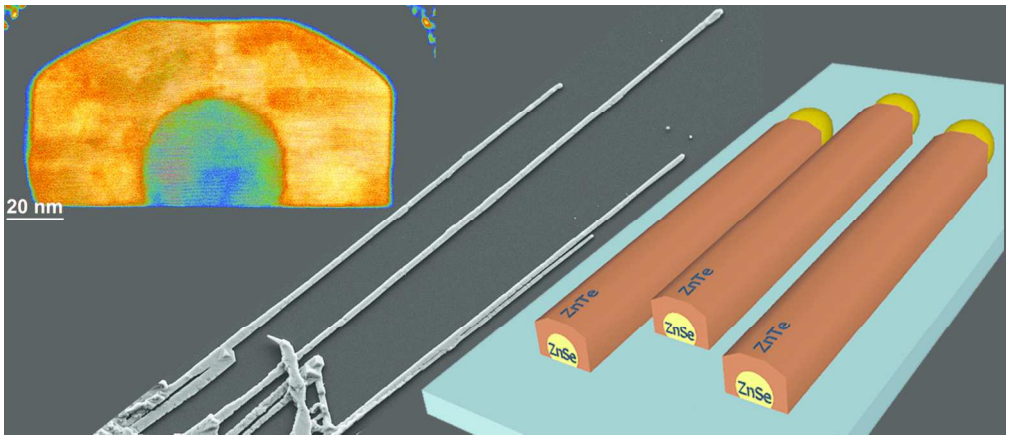

TOC

159x68mm (300 x 300 DPI)

Surface-Guided Core-Shell ZnSe@ZnTe Nanowires as Radial p-n Heterojunctions with Photovoltaic Behavior

Eitan Oksenberg[†], *Sara Martí-Sánchez*[‡], *Ronit Popovitz-Biro*[#], *Jordi Arbiol*[‡,¥] *and Ernesto Joselevich*[†*]

[†]Department of Materials and Interfaces and [#]Chemical Research Support, Weizmann Institute of Science, Rehovot, 76100, Israel.

[‡]Catalan Institute of Nanoscience and Nanotechnology (ICN2), CSIC and The Barcelona Institute of Science and Technology (BIST), Campus UAB, Bellaterra, 08193 Barcelona, Catalonia, Spain

[¥] ICREA, Pg. Lluís Companys 23, 08010 Barcelona, Catalonia, Spain

KEYWORDS: nanowire, planar, epitaxy, ZnSe, ZnTe, optoelectronic.

ABSTRACT

The organization of nanowires on surfaces remains a major obstacle toward their large-scale integration into functional devices. Surface-material interactions have been used, with different

materials and substrates, to guide horizontal nanowires during their growth into well-organized assemblies, but the only guided nanowire heterostructures reported so far are axial and not radial. Here we demonstrate the guided growth of horizontal core-shell nanowires, specifically of ZnSe@ZnTe, with control over their crystal phase and crystallographic orientations. We exploit the directional control of the guided growth for the parallel production of multiple radial p-n heterojunctions, and probe their optoelectronic properties. The devices exhibit a rectifying behavior with photovoltaic characteristics upon illumination. Guided nanowire heterostructures enable the bottom-up assembly of complex semiconductor structures with controlled electronic and optoelectronic properties.

Over the last two decades, single-crystal semiconducting nanowires (NWs) have been the focus of extensive and ongoing research.[1, 2] Their fundamental properties along with increasing control over their dimensions and composition provide a unique combination that is continuously exploited to explore physical phenomena and to test the potential use of nanowires as building blocks for various nanodevices, including electronics,[3] light-emitting diodes (LEDs),[4] lasers,[5] sensors[6] and energy-harvesting devices.[7, 8] Motivated by the prospect of unique properties, enormous efforts were invested in understanding the nuances of nanowire growth in order to ultimately gain control over their dimensions,[9] crystal structure,[10] composition,[11] and modulation of the latter.[12] Interfacing different materials to create nanowire heterostructures can result in electronic, photonic, magnetic, and thermal characteristics that are superior to their bulk or thin-film counterparts.[13] Moreover, their ability to relieve strain radially[13] while maintaining high crystallinity and the flexibility of their growth process enables the creation of unconventional material interfaces with high lattice mismatch.[14]

Nanowire heterostructures, both axial and radial, are being investigated extensively for optoelectronic applications,[15] partly because they enable various degrees of freedom for band engineering. When considering radial heterostructures in particular, different configurations were tailored to fit specific requirements: For a high electron mobility system, a type I core-shell was designed to confine charge carriers in the core region while potentially reducing scattering from the nanowire surface.[16] For LEDs and lasers, multishell radial heterostructures act as confining layers[17] or gain medium[18] respectively. Radial heterostructures can also be engineered to embed single photon quantum emitters.[19] For photovoltaics, type II nanowire heterostructures[20, 21] are promising owing to the large interfacial area of the radial heterojunction, which results in efficient charge generation, separation and transportation.[22]

The integration of nanowires into large-scale optoelectronic systems and probing the performance of many single nanowires for large-scale studies remains challenging due to assembly difficulties.[1] Horizontal single-nanowire devices are usually fabricated using a long, multi-step and often serial process where each device was especially fabricated on a randomly located nanowire.[22-24] Devices based on horizontal arrays of nanowires are few, and usually involve some post-growth assembly method including liquid flow,[25] Langmuir-Blodgett compression[26] and more recently mechanical shearing onto chemically functionalized patterns.[27] Although impressive progress has been made, each method has its drawbacks, which often include length limitations and insufficient control over the alignment and the exact location of both ends of the nanowires. Another common shortcoming is the difficulty to control the directionality and orientation of the nanowires, which is important for applications that require a certain polarity, a directional compositional gradient or axial heterojunctions.

The guided growth approach can offer an advantageous alternative to post-growth methods and facilitate the transition towards large scale single-nanowire research and nanowire-based functional systems.[28] Guided growth exploits epitaxial and graphoepitaxial relationships between the nanowire material and the substrate to guide horizontal nanowires during a vapor liquid solid (VLS) growth, as illustrated in Figure 1A, and bring about well aligned nanowires that grow in specific and reproducible directions and crystallographic orientations.[29] Furthermore, by incorporating a top-down nanolithography process, an array of discrete nanowires with control over their origin, growth direction, crystallographic orientation, and length can be achieved.[30] More than a decade has passed since the first reports on horizontal epitaxial growth of nanowires (ZnO on α-Al_2O_3,[31] In_2O_3 on Si[32] and GaAs on GaAs[33]) and over the last few years a growing number of materials (GaN,[28] ZnO,[29] Sn-doped In_2O_3,[34] InAs,[35] Si,[36] VO_2,[37] TiO_2,[38] SnO_2,[39] ZnSe,[40] ZnTe,[41] InAsSb,[42] $Pb_{1-x}Sn_xTe$[43] and CdSe[44]) were successfully used to grow horizontal nanowires in a similar manner on several substrates (α-Al_2O_3,[28, 40, 41, 44] InAs,[35] Y_2O_3-stabilized ZrO_2,[34] α-SiO_2,[45] SiC,[46] $MgAl_2O_4$[47] and GaN[38]). Despite early concerns that their interactions with the substrate would result in deteriorated crystal quality and optoelectronic properties, guided nanowires showed excellent optoelectronic properties. Moreover, in the case of ZnSe,[40] CdSe[44] and CdS (unpublished data) , photodetectors based on guided nanowires outperformed their vertically-grown counterparts. The latest additions to the horizontal nanowires family, combined with past reports, accumulate to a relatively wide selection of available optoelectronic properties including different band gap energies with either electrons or holes as the majority charge carriers. Despite the growing list of guided nanowires materials and substrates, reports on guided nanowire heterostructures have been scarce,[48] and core-shell horizontal nanowires have not yet been reported.

Here we report the guided growth of horizontally aligned and epitaxial core-shell nanowires with controlled orientation on different flat and faceted planes of sapphire. The n-type core is formed using our recently reported guided ZnSe[40] nanowires and the epitaxial ZnTe p-type shell is inspired by our report of guided p-type ZnTe[41] nanowires. ZnSe and ZnTe are both interesting optoelectronic materials with direct band gap energies in the visible range.[49, 50] Furthermore, theoretical and experimental reports concluded that when the two materials are interfaced, they form a p-n heterojunction with a type II band alignment, which can be exploited for photovoltaics and green electroluminescence.[51-54]

The guided ZnSe@ZnTe core-shell nanowires grow horizontally and aligned as seen in the scanning electron microscope (SEM) image in figure 1B. Their orientation is determined by the interactions between a sapphire substrate and a ZnSe n-type core. In turn, the core acts as an epitaxial template for the overgrowth of a ZnTe p-type shell forming a p-n radial heterojunction as shown in figure 1C. The guided growth was carried out in three general modes that dictate their alignment in reproducible specific directions. The concept and realization of the different growth modes are presented in figure 1D, including: (a) epitaxial growth along specific lattice directions on flat, surfaces and graphoepitaxial growth on spontaneously nanofaceted surfaces along (b) L-shaped nanosteps and (c) V-shaped nanogrooves.

The crystallographic orientation, growth directions and epitaxial relations in this three-material system (sapphire-ZnSe-ZnTe) were characterized and later analyzed in term of strain and strain relaxation mechanisms using geometric phase analysis (GPA). We find that the crystal phase, either wurtzite (WZ) or zinc-blende (ZB), and the crystallographic orientations of the ZnSe core are controlled by its interactions with the flat or faceted sapphire substrates. In almost all cases the ZnTe shell adapts nicely to the ZnSe-sapphire system, through plastic misfit dislocations or a

more complex strain relief process that combines plastic misfit dislocations with elastic plane-bending. The photoluminescence spectra indicate that a type II heterojunction is formed at the core-shell interface of these surface-bound nanowires. To explore their optoelectronic properties, we exploited the deterministic control over their growth direction and fabricated multiple devices in a parallel and simple manner. The devices based on small arrays of nanowires show dark currents below our 10 fA detection limit, but upon illumination they exhibit a clear rectifying behavior with photovoltaic characteristics.

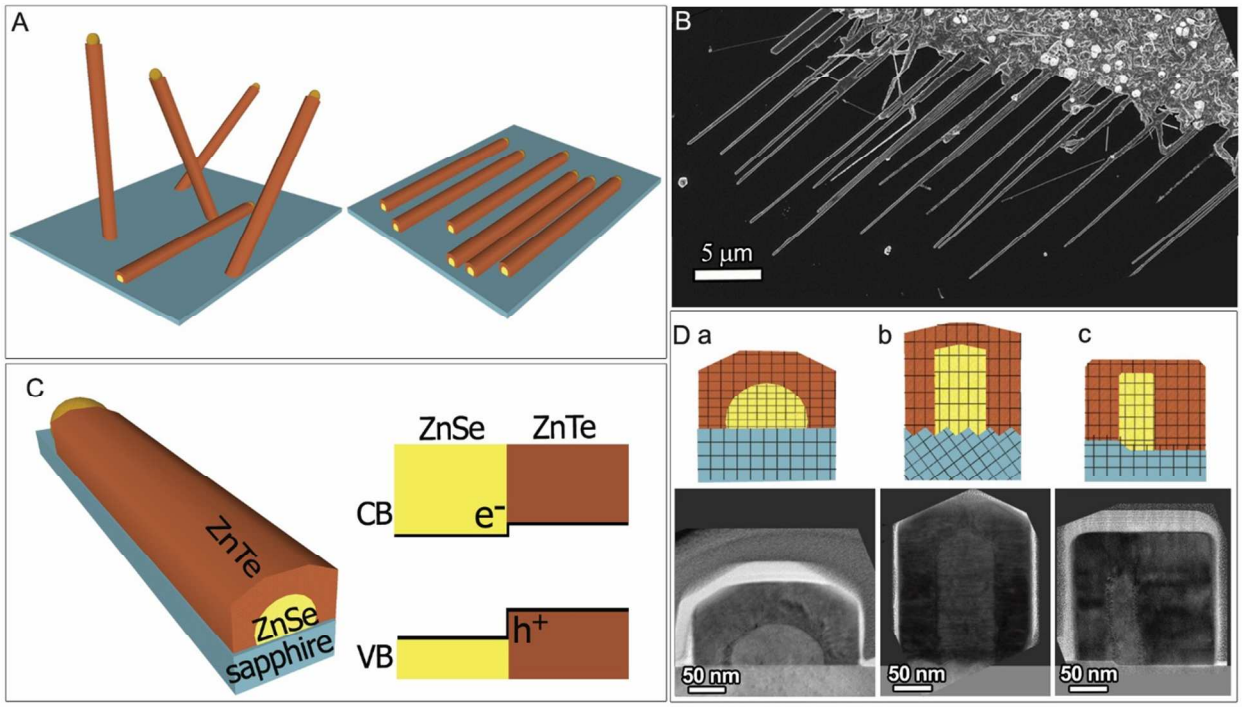

Figure 1. Guided growth of horizontal and aligned ZnSe@ZnTe core-shell nanowires: (A) schematic illustration of guided VLS growth (right) compared to conventional VLS growth (Left). (B) SEM images of guided ZnSe@ZnTe core-shell nanowire arrays grown on C (0001) sapphire. (C) Schematic illustration of a ZnSe@ZnTe core-shell NW and its band diagram. (D) Three modes of guided growth (schematic cross-section views and cross-sectional HRTEM images of their experimental realization): (a) epitaxial growth along specific lattice directions,

(b) graphoepitaxial growth along L-shaped nanosteps of an annealed miscut substrate, and (c) graphoepitaxial growth along V-shaped nanogrooves of an annealed unstable low-index substrate.

RESULTS AND DISCUSSION

We explored the guided growth of ZnSe@ZnTe core-shell nanowires on six different sapphire (α-Al_2O_3) planes. Four flat surfaces: C (0001), A $(1\bar{1}20)$, R $(\bar{1}120)$ and M $(10\bar{1}0)$ for epitaxial growth and two faceted surfaces for graphoepitaxial growth: Annealed miscut C (0001) tilted by 2° toward $[1\bar{1}00]$ with nanosteps, and annealed M $(\bar{1}010)$ with nanogrooves. The VLS growth was carried out in a quartz tube within a three-zone horizontal tube furnace. The system was first purged with a 2% H_2 in N_2 gas mixture and held at a constant 500 sccm flow of the gas mixture while maintaining a 400 mbar pressure for the duration of the process. The gas mixture created a reducing environment and served as the carrier for the elemental Zn, Se and Te that originated from high-purity powders of ZnSe and ZnTe. Islands of Au catalyst were patterned beforehand on the sapphire samples using standard photolithography. Deposition of a thin 1 nm layer of Au followed by dewetting at 550 °C produced patterned islands of Au catalyst nanoparticles. Alternatively, commercial Au nanoparticles were used to catalyze the VLS growth. In the first part of the process, the ZnSe source powder was held at 950-1000°C in the first heating zone of the furnace, while the samples were placed downstream in the second heating zone and held at 720-770°C. After a 15 min growth period, the ZnSe source was replaced with ZnTe *in-situ* using a homemade, magnetically controlled exchange system. Once the ZnTe powder was in place, a second growth period commenced with the powder held at 730°C and the samples at 680°C for 5 min (see Methods and Supporting Information for further details).

Nanowires and nanobelts grow vertically in the center of the Au catalyst pattern while horizontally aligned nanowires grow from the pattern edges where the clean sapphire surface is accessible. The vertical nanostructures can be easily removed by a mild sonication in isopropyl alcohol for a few seconds. When sparsely dispersed Au nanoparticles (10–50 nm) are used as catalyst to gain better control over the catalyst nanoparticle size, the clean sapphire surface is accessible to many more nucleation sites, and under these conditions the horizontal growth is dominant over the vertical growth. The typical total thickness of the horizontal core-shell nanowires varies between 50 and 200 nm. While our growth parameters were adjusted so that the thicknesses of the core and shell are roughly the same, these thicknesses can be adjusted by varying the catalyst size and the duration of each growth period. The length of the guided nanowires can vary from few microns in a short process, and up to 100 μm in a 20 min process. They are slightly tapered and the shell overgrowth is not entirely uniform.

Since the nanowires are bound to the surface, in order to explore their elemental composition, crystallographic structure, epitaxial relations and strain relief mechanisms under a high-resolution transmission electron microscope (HRTEM) and an aberration-corrected scanning TEM (STEM), thin (50-100 nm) slices were cut across and along the nanowires using a focused ion beam (FIB).

Epitaxial guided growth on flat sapphire substrates

On C (0001) sapphire the guided core-shell nanowires grow along the six isoperiodic M $\pm\langle 10\bar{1}0\rangle$ directions, reflecting the threefold symmetry and three glide planes of the substrate (figure 2A). This behavior resembles previous guided growth reports of GaN,[28] ZnO,[29] ZnSe,[40] ZnTe[41] and CdSe[44] nanowires on C-plan sapphire. HRTEM imaging of a cross sectional lamellae

unveil a distinct core-shell structure where both the core and shell are bound to the sapphire substrate. The selected area fast Fourier transform (FFT) of this sapphire-ZnSe-ZnTe architecture reveals clear epitaxial relations between the three materials. Both ZnSe core and ZnTe shell have a ZB crystal structure and their growth axis is along the $[11\bar{2}]$ direction. The planes parallel to the substrate are (111), which are perfectly aligned with the (0006) planes of the sapphire, while their transverse $(1\bar{1}0)$ planes are aligned with the orthogonal $(11\bar{2}0)$ planes of sapphire.

Surprisingly, when examining the guided nanowires on A $(11\bar{2}0)$ sapphire we found a six-directional growth (figure 2B) that resembles the growth we observed on C (0001) (figure 2A). On A $(11\bar{2}0)$ the guided core-shell nanowires grow along two M $\pm[1\bar{1}00]$ directions and 4 S directions $\pm[1\bar{1}01]$ and $\pm[1\bar{1}0\bar{1}]$. The M and S directions are separated by a 61.5° angle while adjacent S directions are separated by a 57° angle. Selected area fast Fourier transform (FFT) of nanowires that grow on A-plane sapphire along the M $\pm[1\bar{1}00]$ directions reveal that they have the same crystallographic behavior as the guided nanowires on C-plane. Both the ZnSe core and ZnTe shell have a ZB crystal structure and their growth axis is along the $[11\bar{2}]$ direction. The epitaxial relations are still clearly observed in the selected area FFT. In this case, the planes that are parallel to the substrate are still (111) despite the fact that the relevant sapphire planes are the $(11\bar{2}0)$ planes and not the (0006) as in the previous case. Accordingly, the transverse planes of the core and the shell are the $(1\bar{1}0)$ planes, which are aligned with the orthogonal (0006) planes of sapphire.

The fact that both on A-plane and on C-plane the nanowires exhibit a six-directional growth with the same crystallographic orientation is peculiar since we generally expect different sapphire planes to induce different growth directions and\or crystallographic orientations for guided nanowires. The growing horizontal nanowires should be inclined to minimize the

interfacial energy and stain that is accumulated during the heteroepitaxial growth. Therefore, in order to better match the different symmetries and atomic structures of the substrates, the preferred growth directions and crystallographic orientation of the growing nanowires is expected to change. In order to shed light on the observed results, it is sufficient to examine more carefully the relations between the sapphire substrate and the ZnSe core since they determine the growth direction and crystallographic orientation of the core and consequently also of the shell. More specifically, we focus on the transverse direction, which was suggested as dominant at determining the crystallographic orientation for guided nanowires in high-mismatch systems.[38]

For guided nanowires on both A and C-plane sapphire, the mismatch at the transverse direction, was relatively high and varied considerably for different sapphire planes and growth orientations (Table S1). A top view of the atomic configuration, of only the topmost unit cell of sapphire and the lowest ZnSe unit cell, implies that a six-directional growth is reasonable on both planes. Taking into consideration these two findings, and assuming a thermodynamically governed growth, it seems that in these conditions the energetic gain of exposing specific facets during the growth is larger than the energy cost of atomic-matching differences. This energetic balance results in the repeating $[11\bar{2}]$ crystallographic orientation, as in this scenario, the fact that the A-plane has an overall structure that encourages a six-directional growth is more important than the atomic structure along those directions.

It is worth mentioning that the behavior of the ZnSe-sapphire system reported herein is different than that reported in our previous work.[40] Many reports in the literature, including our own, demonstrate changes in epitaxial growth of nanowires due to changes in the growth parameters.[55] We believe that our recently assembled growth system, and resulting changes in the growth conditions, are responsible for the different result in this work compared to our

previous study. We find that different guided growth regimes can be observed, in a reproducible matter, within the same ZnSe-sapphire system as a result of different growth parameters. This might suggest that depending on the growth conditions, at least with some material systems, there is not one, but several guided growth behaviors that could be individually addressed. Perhaps different conditions tilt the energetic balance towards specific growth behaviors in a thermodynamically governed process. Otherwise, the different behaviors can be kinetically controlled, as it is known that certain facets form faster than others even when they are not thermodynamically more stable.[56] In any case, this suggests that a high-resolution control over the growth conditions can bring about adjustable guided growth, where one can choose the best suited direction and crystallographic orientations for a specific application.

The ZB $[11\bar{2}]$ and the WZ $[10\bar{1}0]$ crystallographic growth directions are almost identical when observed through only a selected area FFT of the cross section. In order to differentiate between the two, and determine unambiguously the growth axis of the guided nanowires, lamellae along the growth direction of guided nanowires on both sapphire planes were prepared. The HRTEM images and analysis for a guided nanowire on A-plane is presented in figure 2C along with energy filtered TEM (EFTEM) that discloses the expected locations of the different elements in the nanowire. The selected-area FFT confirmed the ZB $[11\bar{2}]$ growth direction since the orthogonal direction was clearly the ZB $[1\bar{1}0]$ direction for the ZnTe shell. Since the lamella was thicker than the core, a moiré pattern was formed where the ZnSe and ZnTe lattices overlap. It was still possible to determine the ZB $[1\bar{1}0]$ of the core from the FFT and the moiré periodicity. The lamella along a nanowire on C-plane can be found in figure S2A along with moiré periodicity calculations.

Further atomic-resolution aberration-corrected HAADF STEM analyses obtained on the lamellae cut along the guided nanowires growth direction on A-plane confirmed the ZB structure for both the core and the shell (Figure S3). In addition, the crystal polarity of the nanowire could be extracted from the HAADF-STEM images[57] confirming that the NW is B-polar (Se/Te or anion polar) along the guided growth direction and A-polar (Zn or cation polar) in the vertical direction from the substrate. The B-polarity along the guided growth direction is in good agreement with the usual polarity observed in vertically grown ZnTe NWs.[57, 58]

Once the crystallographic orientation and polarity of the core and shell are known, we can also gain insight into the morphology of the shell and its mechanism of formation. During our efforts to find the growth parameters for the desired morphology and thickness of the shell overgrowth, we observed some extreme cases ranging from a massively thick shell to an incomplete shell growth (figure S4a). Even at our optimized condition for shell overgrowth on C and A-plane sapphire, it is clear that the shell overgrowth is not entirely uniform (figure S4b). The results containing an incomplete shell and HRTEM images from the lamellae cut along the axis of the nanowire with a continuous shell (figure 4Sc-d) imply that our shell formation resembles the previously reported Plateau–Rayleigh crystal growth.[59] The epitaxial shell nucleates in several nucleation centers along the nanowire and, given the right parameter, the centers grow along the nanowire and merge to form a continuous shell. This mechanism is further discussed in the Supporting Information.

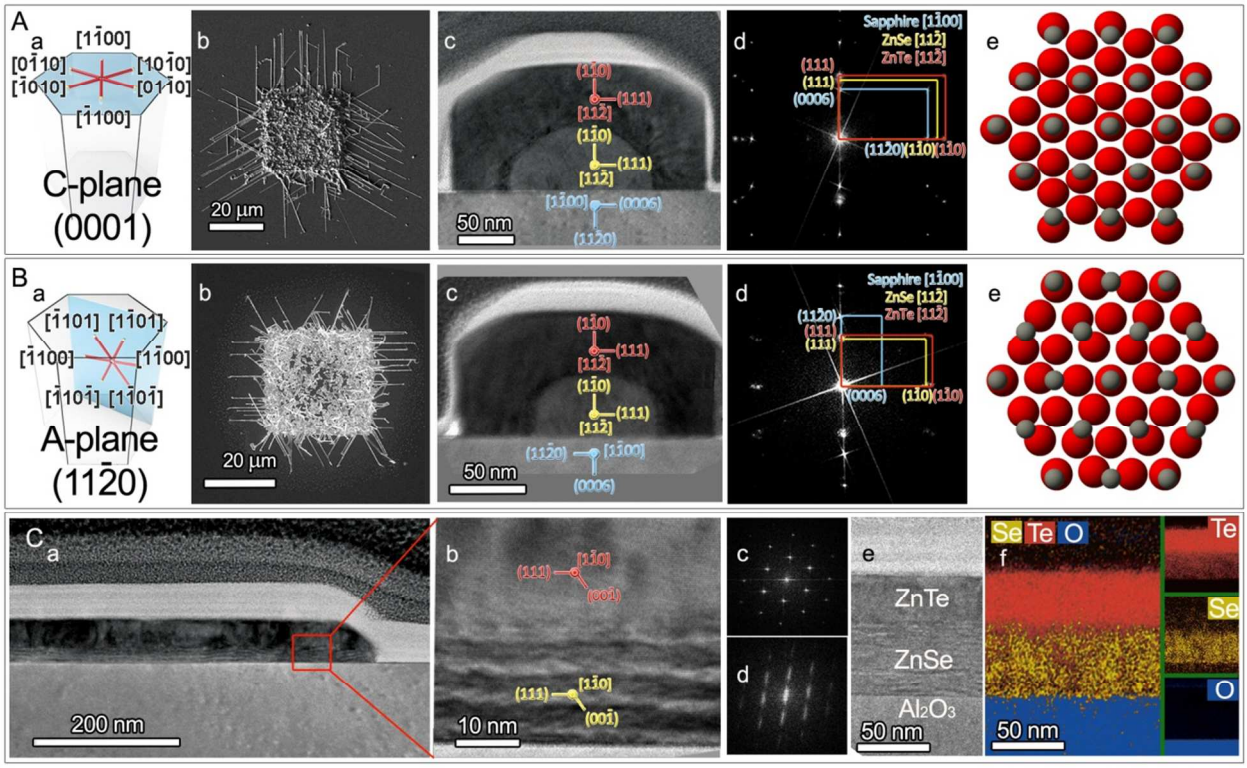

Figure 2. Guided growth of epitaxial core-shell nanowires on C-plane and A-plane sapphire. (A-B) For each substrate: (a) A schematic illustration of the plane and directional growth. (b) SEM image of the guided Nanowires. (c) HRTEM cross-section image, marked with the crystal planes and direction of the nanowire ZnSe core (yellow), ZnTe shell (red) and the sapphire substrate (blue). (d) Selected area fast Fourier transform (FFT) of the cross section image. (e) Top view of the atomic crystal structure, of only the topmost unit cell of sapphire and the lowest ZnSe core unit cell. (C) Analysis along a guided nanowire on A-plane sapphire: (a) HRTEM cross-section image. (b) Larger magnification of the indicated area marked with the crystal planes and direction of the nanowire ZnSe core (yellow), ZnTe shell (red). Selected area fast Fourier transform (FFT) of (c) the ZnTe shell and (d) the ZnSe core. EFTEM analysis with (e) zero loss image and (f) an elemental map overlay and the Se, Te, and O elemental maps.

The guided growth of our core-shell nanowires on R $(1\bar{1}02)$ sapphire is predominantly along two non-isoperiodic directions of the sapphire substrate, $[\bar{1}101]$ and $[\bar{1}3\bar{2}2]$ as depicted in figure S5. Lamellae were cut for both growth directions. Despite growing along non-isoperiodic directions, all nanowires presented the same WZ crystal structure with the same $[\bar{4}223]$ growth direction both for the ZnSe core and ZnTe shell. The nanowires had a trapezoid form with distinct $(01\bar{1}0)$ and $(1\bar{1}02)$ facets and it is quite noticeable that the ZnTe shell is not isotropic and grows preferably over the $(1\bar{1}02)$ planes of the ZnSe core. Further manipulating the growth conditions can lead to a completely facet selective growth. On flat M $(10\bar{1}0)$ sapphire we observed more unusual growth directions. The guided core-shell nanowires grow along $\pm[1\bar{2}10]$, $\pm[\bar{1}2\bar{1}\bar{3}]$, and $\pm[\bar{1}2\bar{1}6]$ directions of the sapphire substrate (figure S5). The analyzed nanowires have a WZ crystal structure and grow along the polar [0001] direction. The unusual phenomena observed with R-plane and M-plane, including the anisotropic shell growth and the growth along multiple relatively rare and different crystallographic orientations, are further discussed in the Supporting Information.

Graphoepitaxial guided growth on faceted sapphire substrates

One of the strengths of the guided growth approach is the ability to control the growth direction of the horizontal nanowires through surface manipulation. Past studies have shown that nanowires can grow along nanosteps and nanogrooves on nanofaceted sapphire substrate.[23, 24, 40-42] This mode of guided growth, which we refer to as graphoepitaxy, has proven to be dominant over epitaxial growth, and essentially overrules the epitaxial relations between the sapphire and the nanowire.[28, 29, 40, 41, 44] This was the case also for the core-shell guided nanowires, as can be seen in figure 3. The six-directional growth of guided nanowires on flat C-plane is overruled by annealing a C (0001) sapphire substrate that was miscut 2 degrees towards $[1\bar{1}00]$ to form an

array of L-shaped nanosteps due to step-bunching of the high-index.[60] The nanowires in this case are guided by these nonosteps and grow along them to the ±[$1\bar{2}10$] directions of the sapphire substrate (figure 3A). Despite nice alignment along specific sapphire directions, these nanowires are more ragged than the nanowires grown on flat substrates. Furthermore, unlike the very homogeneous crystallographic structure observed on flat substrates, the nanowires that grow along the nanosteps have a variety of crystallographic orientation and crystal phases (figure S6 and table S2).

Flat M (1010) sapphire is thermodynamically unstable. Annealing at elevated temperatures (*e.g.*1600°C) causes surface restructuring and the more stable S-plane and R-plane facets create well-structured periodic nanogrooves.[60] The horizontal core-shell nanowires grow along the two ±[$1\bar{2}10$] directions of the nanogrooves instead of the six directions of flat M ($10\bar{1}0$) sapphire (figure 3B). Similar to the findings on a miscut C-plane, the guided core shell nanowires that grow in the graphoepitaxial growth mode were more ragged, and presented a few different cross-sectional structures with some variation of crystallographic orientations and crystal phases.

In a previous work,[40] we mentioned that graphoepitaxial nanowires need to adapt simultaneously to two sapphire planes and their energetic constraints. We hypothesized that the accumulated strain is manifested in a rougher surface and lesser uniformity in growth axes. In the present case, since the shell growth is a vapor-solid (VS) growth, it is highly influenced by the initial smoothness of the guided core. Small imperfections and roughness in the core can be highlighted when the shell forms and the end result is often bulky. With that said, some of the guided nanowires have high aspect ratio and faceted rectangular cores exposing smooth lateral facets, which proved ideal as templates for the shell growth (figure S6 and table S2).

The guided growth of horizontal core-shell ZnSe@ZnTe nanowires on all these different substrates extends the generality of the approach to nanowire heterostructures while providing further empirical data toward its understanding. Although the exact mechanism of guided growth is not yet fully elucidated, a few models have rationalized the horizontal growth of nanowires, either by considering a fully faceted limit of a continuum model taking into consideration facet dynamics, droplet statics, and the energy required to introduce a new facet,[61] or by introducing thermal fluctuations to a thermodynamic description.[62] Hopefully the growing empirical database along with other, more recent, reports including those exploring the Gibbs-Thomson effect in horizontal nanowires[63] and the VLS etching of surfaces by running gold nanodroplets[64] will accumulate to a comprehensive understanding of this phenomenon.

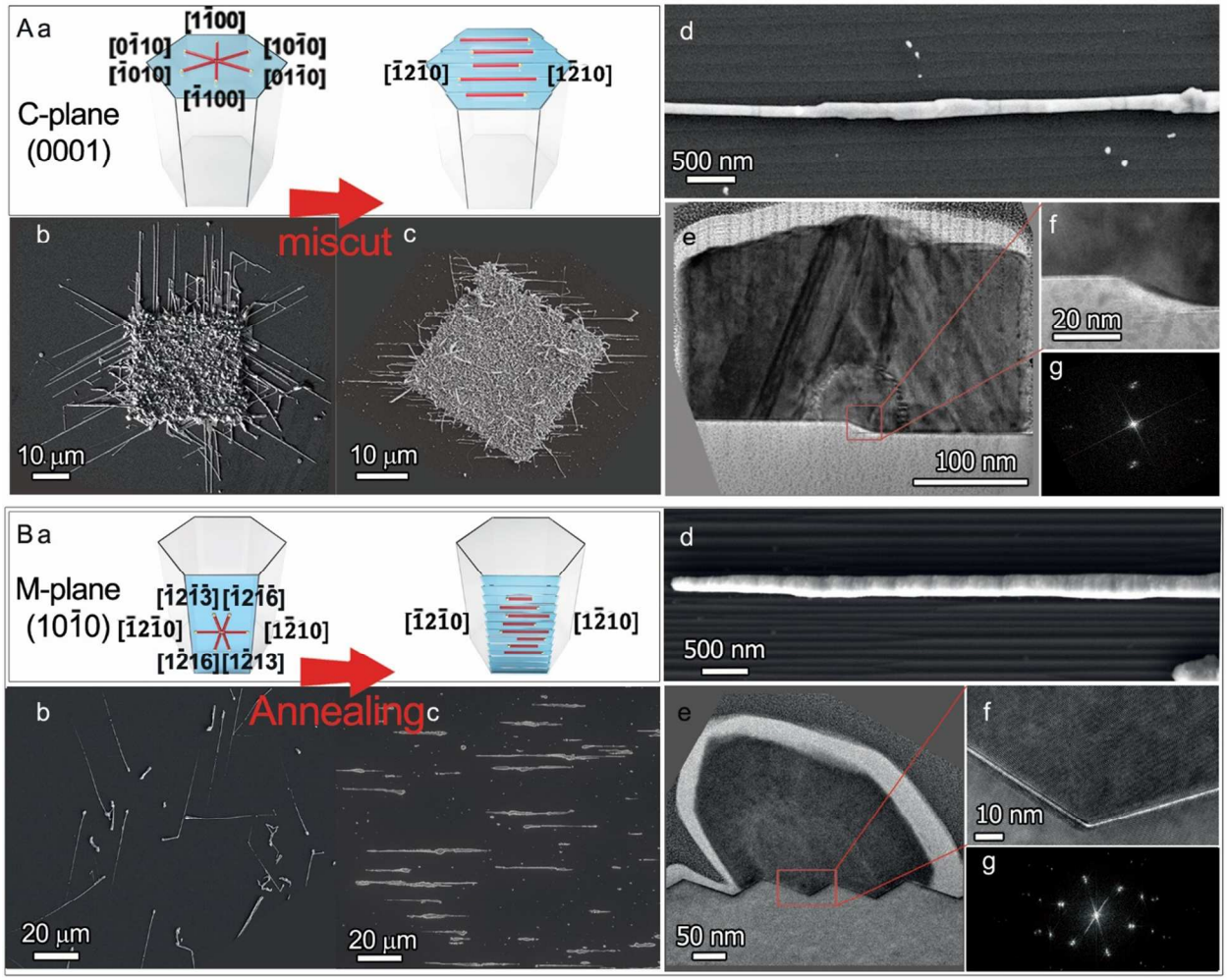

Figure 3. Graphoepitaxial growth of ZnSe@ZnTe core-shell guided nanowires on (A) C (0001) sapphire (well-cut vs miscut) and (B) M $(10\bar{1}0)$ sapphire (non-annealed vs annealed). For each substrate: (a) A schematic illustration of the epitaxial and graphoepitaxial growth directions. SEM images of the guided nanowires on (b) flat and (c) faceted substrates. (d) A higher magnification SEM image revealing the nanofaceted surface. (e) Cross-sectional HRTEM images of the guided Nanowires and the substrate. (f) High magnification image of the nanowire-substrate interface and (g) the selected area Fourier transform of the NW.

Stress relief mechanisms in guided core-shell nanowires

During the shell formation, a complex stress relief mechanism is taking place in order to minimize the elastic energy on the two mismatched material systems. From Fourier analysis on the atomic-resolution aberration-corrected HAADF-STEM micrograph in Figure 4(a) we can notice a triple spot instead of the double core-shell spot expected. One spot corresponding to the ZnSe planes of the core, and a double spot arising from the shell. This double spot corresponds to equal plane spacings, but, as a result of plane bending, there is a 4º angle between the planes on the left part and the right part of the shell.

Through geometrical phase analysis, the dilatation and rotation maps of ZnSe@ZnTe (111) planes have been obtained. By keeping the core as a reference, we can measure a mean dilatation of 8.8 % in shell plane spacing, which is higher than the expected 7.4 % (for a perfectly relaxed ZnSe@ZnTe), indicating tensile strain on the shell structure. More information can be obtained from the rotation map, where we observe both plastic and elastic strain relaxation mechanisms.[65, 66] A set of misfit dislocations in the vertical planes are visible (white arrows in Figure 4e), showing a plastic strain relaxation while at the same time we observe a general rotation on planes at both sides of the shell with a mean value of +2º (right side shell planes) and -2º (left side shell planes) which are consistent with the rotations measured in the FFT. This plane bending phenomena seem to dramatically depend on the core morphology, observing lower angles when the core surfaces are flatter. Further study on the relaxation mechanisms on the different structures depending on core morphology and substrate orientation will be performed in the future.

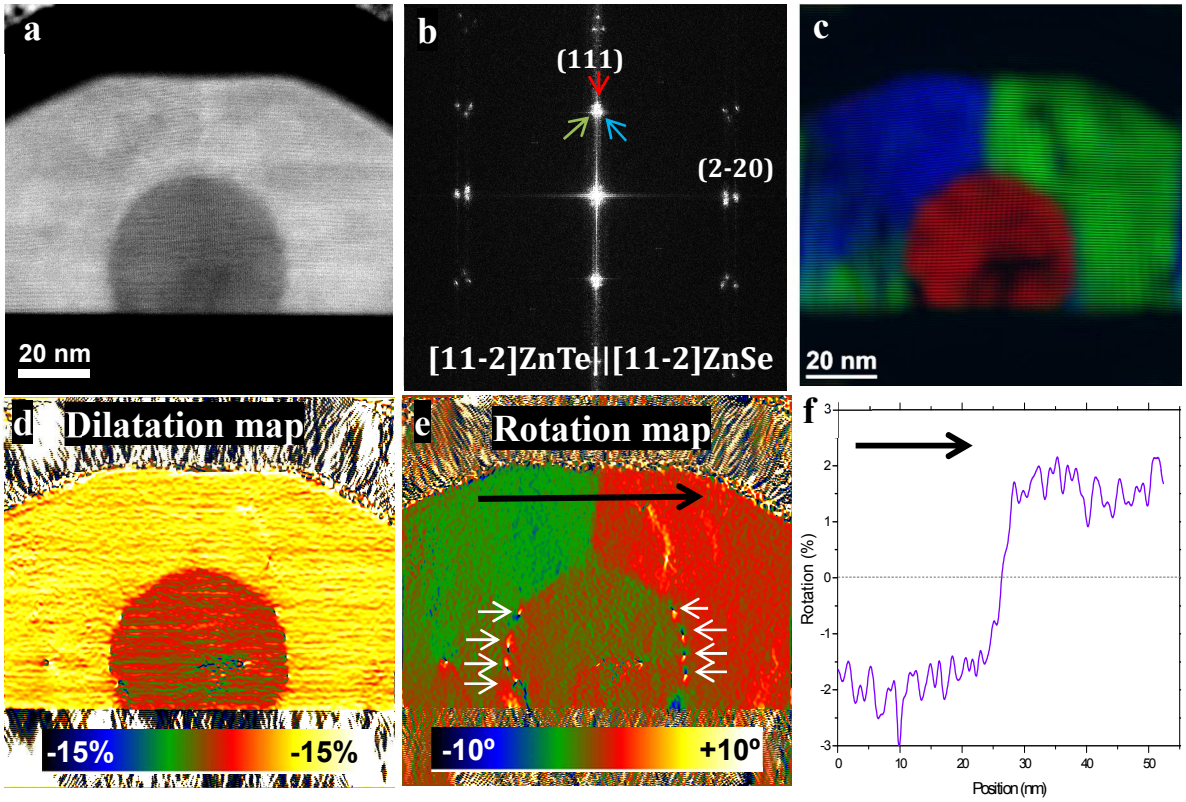

Figure 4. (a) Cross-sectional atomic resolution HAADF-STEM micrograph of a guided ZnSe@ZnTE core-shell nanowire along sapphire A-plane and (b) its corresponding FFT. (c) Structural map obtained by filtering the spots of the FFT. (d) Dilatation and (e) rotation maps obtained through Geometrical Phase Analysis (GPA) along the ZnSe and ZnTe (111) planes. (f) Rotation profile obtained along the arrow indicated in (e). White arrows in (e) point to the misfit dislocations.

Optical properties of the guided ZnSe@ZnTe core-shell nanowires

Room-temperature photoluminescence (PL) spectra were obtained with a micro-Raman system (Horiba LabRAM HR Evolution) using a 325 nm He-Cd laser. In order to compare the optical behavior of the core-shell system with its individual components, we measured the PL spectra of single ZnSe and ZnTe guided nanowires that were grown separately in the above mentioned

growth conditions. PL measurements of the ZnSe@ZnTe core-shell guided nanowires were conducted as well (figure 5). The typical PL spectrum of a single ZnSe guided nanowire on C (0001) sapphire had only one narrow peak at 459 nm (~2.7 eV) that corresponds to the near-band-edge (NBE) emission. For ZnSe, another broad deep-level (DL) emission peak centered at 635 nm (1.95 eV) is often observed and attributed to intrinsic point defects (IPDs),[67] the lack of this defect band in our measurements indicates a high crystal quality of the ZnSe core. The case of a typical ZnTe guided nanowire on C (0001) sapphire was similar, with one narrow peak at 549 nm (~2.26 eV) that corresponds to its NBE emission. Notably, a common broad DL emission peak centered at 670 nm (1.85 eV) due to IPDs is not observed.[41]

The typical PL spectrum of a single ZnSe/ ZnTe core-shell guided nanowire on C (0001) sapphire has a sharp peak at 461 nm which corresponds to the ZnSe NBE emission with a 2 nm red shift. The second broad peak, with a dominant peak and a strong shoulder, was fitted to 3 Gaussians, one with a distinctive peak at 546 nm, and two that comprise the shoulder. We attribute the peak at 546 nm to the NBE emission of the ZnTe shell. Notably, this peak is broader and about 3 nm blue-shifted compared to the emission of the guided ZnTe nanowires. We suspect that the small shifts in the NBE emission of ZnSe and ZnTe might originate from the strain induced by the formation of the core-shell structure. Furthermore, the broadening of the NBE emission is possibly due to strain inhomogeneity along or across the growth axis of the nanowires. Within the shoulder, there is one low-intensity Gaussian at 597 nm and a higher intensity one at 612 nm (see figure S7).[68] As for the orange emission at 597 nm and 612 nm, we have to consider two possible causes, either a DL emission that originates from the formation of IPDs during the shell growth or a type II recombination emission.

When considering the formation of IPDs as a possible origin of the orange emission at 597 nm and 612 nm, one should take into account the commonly formed DL emissions for the corresponding materials. For ZnSe, the common DL emission is around 635 nm and for ZnTe around 670 nm. For both materials the common DL emission wavelengths are longer than those observed in the spectrum (612 nm). Thus even if we assume that IPDs are formed during the shell growth, it is still unlikely that they are responsible for the orange emission that is observed in the guided ZnSe@ZnTe core-shell nanowires. A different possible origin of the orange emission is a type II recombination at the ZnSe-ZnTe heterojunction between electrons from the conduction band of the ZnSe core and holes from the valence band of the ZnTe shell (figure 1C). Theoretical calculations and experimental data show that the n-type ZnSe and p-type ZnTe form a type II p-n heterojunction. The energy gap between the ZnSe conduction band and the ZnTe valence band is estimated at ~2.0 eV[52-54, 69] (620 nm), which is close to the 612 nm emission peak that we observe in the orange emission shoulder. The slight shift can be attributed to strain as a result of epitaxial mismatch that could modulate the band structure.[70] In principle, time-resolved PL at low temperatures could establish the origin of the orange emission.[68] However, these measurements were not possible with our current setup, and are hence beyond the scope of this report. In any case, considering the electronic nature of these materials and the fact that common DL emission band of ZnSe and ZnTe do not match the observed orange emission, this is most likely a type II recombination.

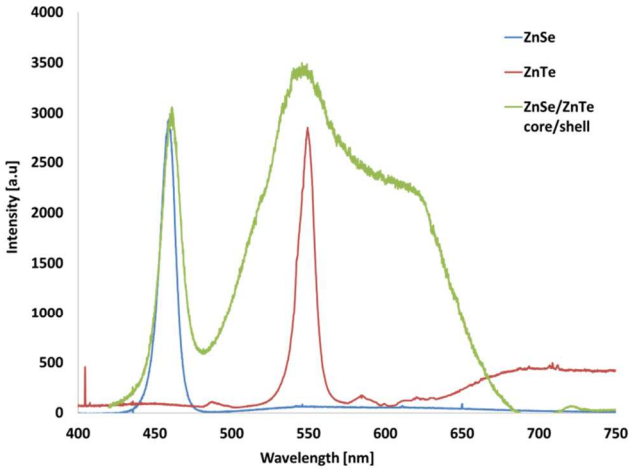

Figure 5. Room temperature PL spectra of single ZnSe (blue), ZnTe (red) and ZnSe@ZnTe core-shell guided nanowires (green) on a sapphire substrate. The peak at 460 nm corresponds to the NBE emission of ZnSe, the peak at 549 nm corresponds to the NBE of ZnTe. The orange emission around 600 nm that causes the shoulder in the core-shell spectrum is attributed to type II recombination.

Optoelectronic properties of the guided ZnSe@ZnTe core-shell nanowires

Previous studies conducted on guided nanowires concluded that despite early concerns, the substrate-nanowire interactions do not cause deterioration in the crystal quality and the optoelectronic properties of the nanowires.[40, 41, 44] On the contrary, guided nanowires usually show excellent optoelectronic properties. In the case of ZnSe,[40] CdSe[44] and CdS (unpublished data), photodetectors based on guided nanowires outperformed their vertical counterparts. This work demonstrates core-shell nanowires that are guided through surface-nanowire interactions. In this configuration, the ZnSe core and ZnTe shell are expected to form a radial p-n heterojunction, therefore, probing the optoelectronic behavior of this system is essential for its understanding.

In order to probe the optoelectronic properties of the core-shell guided nanowires we exploited the deterministic control over their location and growth direction and fabricated multiple devices using only parallel fabrication steps. The growth of the guided core-shell nanowires, as described earlier, resulted with a completely covered core. However, in order to probe the radial heterojunction, one electrode should be in contact with the p-type shell while the other one should be connected to the n-type core. ZnSe and ZnTe are very similar chemically hence selective etching to expose part of the core was not perused. Instead, we formulated a fabrication process where certain segments of the core are masked prior to the shell growth in order to have them accessible to direct contact with an outer electrode, as illustrated in figure 6. In this scheme, after the growth of a guided ZnSe core as described earlier, standard photolithography and electron-beam evaporation of a 200 nm SiO_2 protective layer was carried out on part of the core. Next the shell was grown, followed by wet etching of the protective layer. The final step was patterning and depositing Ti/Au electrodes (10 nm/90 nm), again with photolithography and electron-beam deposition so that one electrode contacted the bare ZnSe core while the other one contacted the shell (see methods for further details). In this manner, multiple devices were fabricated using only parallel fabrication steps. Alternatively, the photolithography steps can be replaced with e-beam lithography steps for better control over the dimensions and location of the contacts. The number of nanowires in each device is determined by the yield of the ZnSe core growth and the catalyst size. The yield can vary with the growth parameters while the catalyst size is determined by the photolithography process. As shown in figure 6B-D, a device that was fabricated in this manner has between 1 and 15 core-shell guided nanowires that cross a 2-8 um gap between the electrodes. A typical cross-section of the nanowires is 50 nm and 150 nm for the

core and core-shell structure respectively. Energy-dispersive X-ray spectroscopy (EDS) mapping validates that within the gap the ZnSe core is partly covered with the ZnTe shell.

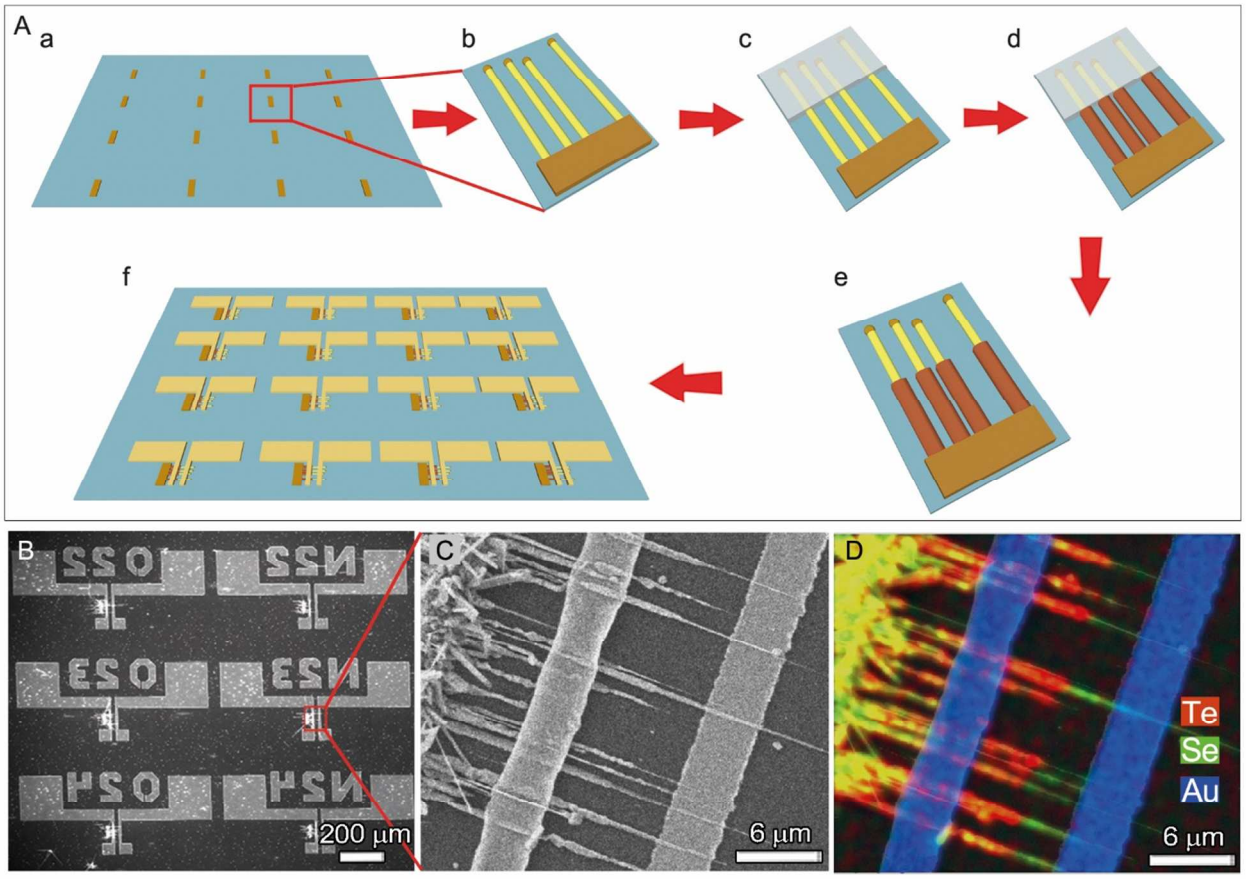

Figure 6. Parallel fabrication of multiple devices based on ZnSe@ZnTe Core-shell guided nanowires (A) Schematic illustration of the fabrication steps: (a) catalyst islands deposition followed by (b) ZnSe guided core growth, (c) protective shell deposition and (d) ZnTe shell growth before (e) etching of the protective layer and (f) deposition of electrodes. (B) SEM image of a typical array of devices. (C) Magnification of a single device and its (C) SEM-EDS elemental mapping.

Once the devices were fabricated, we probed the optoelectronic properties of the guide core-shell nanowires using a Janis ST-500 probe system with a Keithley 4200-SCS. *I-V* measurements were done under vacuum, at room temperature, in dark condition (16 µW/cm^2 ambient light) and

under a 405 nm laser illumination at different intensities. In figure 7 a typical device with 9 parallel core-shell nanowires can be seen along with its 3D height map and current-voltage (*I-V)* curves. The devices exhibit very low dark currents as our 10 fA detection limit was not sufficient to measure a current in dark conditions. This is not surprising considering our previous report on dark currents below our 10 fA detection limit in photodetectors based on ZnSe guided nanowires.[40] However, under illumination of 0.7 mW/cm^2 *I-V* curves could be measured due to the generated photocurrent, and a rectifying behavior was observed as expected for a p-n heterojunction diode. Furthermore, an open-circuit voltage of ~0.3V was measured and a short-circuit current of ~2 pA. Due to the extremely low dark current, only the lower limit of the on/off ratio and responsivity can be determined when assuming the dark current is at the 10 fA noise level. The responsivity is defined as $R_\lambda = \Delta I/PS$. where, ΔI is the difference between the photocurrent (I_{photo}) and dark current (I_{dark}), P is the laser power density, and S is the effective illumination area estimated by the electrode gap, nanowires diameter and number of nanowires. The lower bound responsivity of this device is estimated at 0.2 A/W at zero bias. When the *I-V* measurements were conducted under increasing illumination intensities (figure 7D), the magnitude of the short-circuit current increased linearly while the open-circuit voltage remained approximately constant. In principle, this core-shell p-n heterojunction should exhibit electroluminescence, which would provide further information about its band alignment and deep level states. However, using our commercial micro-Raman/PL system, we did not detect any measureable electroluminescence. One possible reason for the low intensity of electroluminescence is the very low dark conductance of the ZnSe nanowires.

The performance of a device or an array of devices can be adjusted in relative ease by changing the number of nanowires in each device. This can be achieved by changing the size of the catalyst pattern and creating larger devices, or by varying the growth parameters to receive different yields. The ability to fabricate simultaneously a large number of devices based on one, several or many core-shell nanowires with a radial heterojunction in the same crystallographic orientation can be used as a powerful tool for both research and applications.[71]

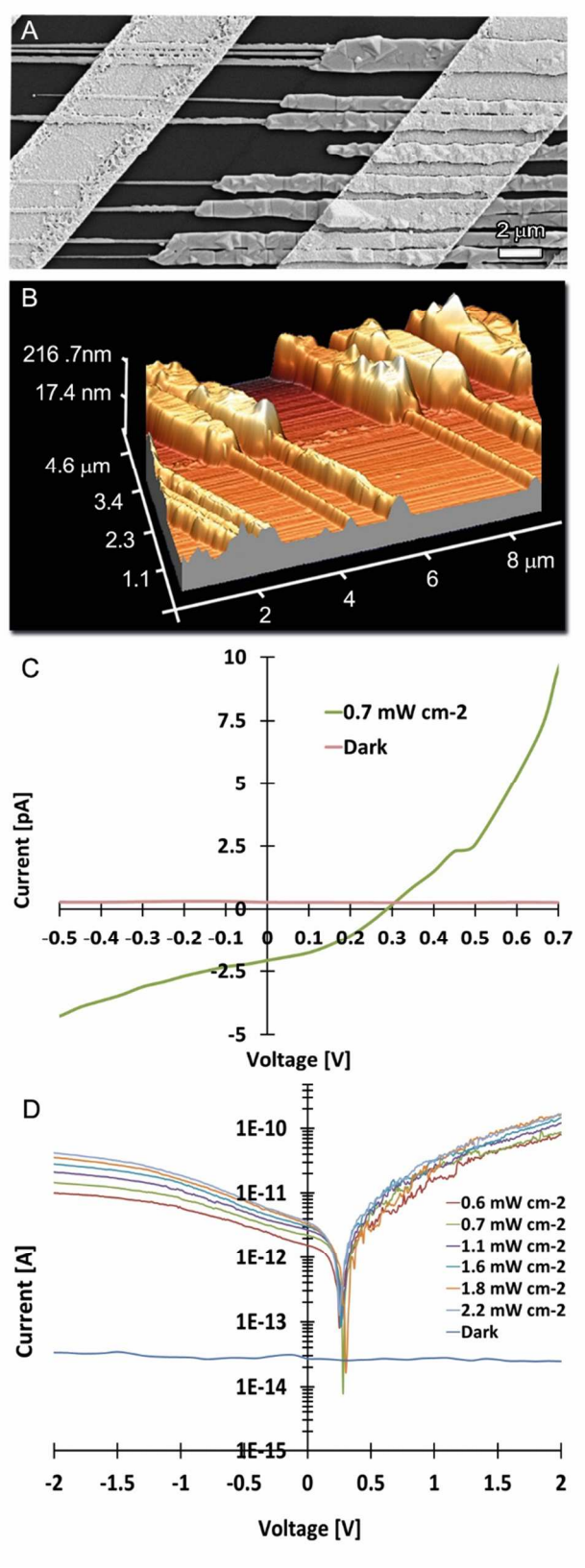
A
2 µm
B
216 .7nm
17.4 nm
4.6 µm
3.4
2.3
1.1
2
4
6
8 µm
C
0.7 mW cm-2
Dark
Current [pA]
Voltage [V]
D
0.6 mW cm-2
0.7 mW cm-2
1.1 mW cm-2
1.6 mW cm-2
1.8 mW cm-2
2.2 mW cm-2
Dark
Current [A]
Voltage [V]

Figure 7. Optoelectronic behavior of guided ZnSe@ZnTe core-shell nanowires devices (A) SEM image of a typical device. (B) Its 3D AFM height map (C) *I-V* curve in dark condition (16 μW/cm^2 ambient light) and under 0.7 mW/cm^2 illumination of a 405 nm laser (C) logarithmic *I-V* characteristics different illumination intensities.

CONCLUSIONS:

In summary, we have demonstrated the guided growth of horizontal core-shell nanowires, specifically ZnSe@ZnTe with controlled orientation on six different flat and faceted planes of sapphire (Table S3, Supporting Information). Both epitaxial growth along specific lattice directions on flat surfaces and graphoepitaxial growth along nanosteps and nanogrooves were realized. We analyzed the crystallographic orientations and stress relief mechanisms of the guided core-shell nanowires. The crystal phase, either wurtzite or zinc-blende, and crystallographic orientations of the core and shell are controlled by the substrate that is selected and the growth conditions. The ZnSe-sapphire epitaxial and graphoepitaxial relations and the resulting core crystallographic orientation determine the shell behavior which adapts to the atomic structure of the core through a combination of plastic misfit dislocations and elastic plane-bending strain-relief processes.

We exploited our deterministic control over both the growth direction and the crystallographic orientation of the guided nanowires to fabricate multiple devices using only parallel steps. The devices based on small arrays of nanowires with a radial p-n heterojunction show dark currents below our detection limit of 10 fA. Upon illumination, the devices exhibit a rectifying behavior with photovoltaic characteristics and currents up to 5 nA (under a 405 nm, 2.5 mW/cm^2 illumination and 2 V forward bias). The simultaneous fabrication of a large number of devices

based on one, several or many nanowires in the same crystallographic orientation can be utilized for statistical research or applications that require easy fabrication and scalability.

The B-polar (Se/Te polar) atomic configuration along the growth direction, implies that nanowires that grow along a certain sapphire direction will have the same polarity. Therefore the guided growth can yield homogenous arrays of nanowires with the same polarity, which would be highly beneficial for polar sensitive applications. The introduction of guided nanowire heterostructures could enable the production of many complex semiconductor structures with controlled electronic and optoelectronic properties not available by other means.

METHODS:

ZnSe@ZnTe core-shell guided nanowires synthesis. The substrate preparation and catalyst deposition and patterning are describe previously[29] and illustrated in the figure S1 in the Supporting Information. The VLS growth was carried out in a three-zone horizontal-tube furnace. The quartz tube reactor was purged with a N_2 (99.999%, Gordon Gas) and H_2 (99.99995%, Parker Dominic Hunter H_2-generator) 49:1 mixture and kept 400 mbar with a constant 500 sccm flow of the N_2/H_2 mixture. In the first part of the process, the ZnSe source powder (99.99% SPI Supplies) was held at 950-1000°C in the first heating zone of the furnace, while the samples were placed downstream in the second heating zone and held at 720-770°C. After a 15 min growth period, the furnace was moved so that the source and the sample are not heated. The furnace temperatures were set to 730°C at the first zone and 680°C at the second heating zones and using a home built magnetic crucible holder the ZnSe powder was pulled away and replaced with a ZnTe powder (99.99% Sigma-aldrich). Once the furnace reached the

desired temperatures, it was moved over the sample and ZnTe powder to enable the 5 min shell growth.

Structural characterization. The nanowires were imaged with a scanning electron microscope (Supra 55VP FEG LEO Zeiss). In order to analyze the crystallographic structure and orientations of the nanowires and substrate, a focused-ion beam (FIB, FEI Helios 600 Dual Beam microscope) was used to cut thin (50-100 nm) lamellae across or along the nanowire, which were later inspected under a high-resolution transmission electron microscope (HRTEM, FEI Tecnai F30). The HRTEM images were analyzed using fast Fourier transform (FFT) from selected areas across the nanowire, and the FFT peaks were fitted to the crystallographic tables of bulk ZnSe, ZnTe and sapphire. The core-shell nanostructures were also studied by atomic resolution high angle angular dark-field scanning transmission electron microscopy (HAADF-STEM) using a probe corrected FEI Titan 60−300 equipped with a high brightness field emission gun (XFEG) and a CETCOR corrector from CEOS. The obtained data allowed us to perform geometric phase analyses (GPA) for strain measurements.[72]

Optical characterization. Photoluminescence (PL) measurements were done using a micro-Raman/micro-PL system (Horiba LabRAM HR Evolution). A 325 nm He-Cd laser was focused on the nanowire through a reflective 70X objective lens. The PL signal was collected using the same objective and sent to a 300 lines/mm grating and an EMCCD camera.

Device fabrication and optoelectronic characterization. After guided growth of the ZnSe core, the sample was removed from the growth reactor. A photolithography mask compatible with the catalyst pattern was used to define 0.01 mm^2 squares that for the 200 nm SiO_2 protective layer that was deposited using e-beam deposition. The samples were cleaned in Acetone, IPA

and DI water before they were dried in N_2 and inserted into a clean reactor for the ZnTe shell growth. The shell growth is as described above with a prior step where the samples were heated at 730°C for 1 min in the 2% H_2 in N_2 atmosphere to remove oxides that could form between the two crystal growth steps. After the shell growth the protective layer was etched in 6:1 buffered oxide etch. Ti/Au (10/90 nm) source/drain electrodes were patterned using photolithography and deposited over the shell and core of the guided nanowires, separated by 2 or 8 μm gaps. Optoelectronic measurements were done under vacuum at room temperature using a Janis ST-500 probe system with a Keithley 4200-SCS. The electrical measurements were done in dark condition (16 $\mu W/cm^2$ ambient light). For optoelectronic measurements we used a 405 nm laser diode module (Laser Components) to illuminate the device with power controlled by a metallic neutral density filter (Thorlabs). The light intensity was calibrated with a LM-2 VIS silicon photodiode optical sensor (Coherent).

ASSOCIATED CONTENT

Supporting information: (1) Synthesis system illustration (2) Lattice mismatch calculations for A $(11\bar{2}0)$ and C (0001) sapphire. (3) Lamella along a nanowire on C-plane and moiré periodicity. (4) Polarity determination along the growth axis of the nanowires and discussion of its implications (5) shell morphology and formation discussion (6) Epitaxial growth on M-plane and R-plane. (7) Variation in the cross sections and orientations of guided core-shell nanowires on faceted surfaces. (8) Summary of epitaxial relations on different sapphire planes. (8) Gaussian fit of the photoluminescence spectrum of core-shell guided nanowires.

AUTHOR INFORMATION

Corresponding Author

**E-mail: ernesto.joselevich@weizmann.ac.il

Funding Sources

The Israel Science Foundation 1493/10, Minerva Stiftung (project No. 711138), European Research Council (ERC) Advanced Grant (No. 338849).

Notes

The authors declare no competing financial interest.

ACKNOWLEDGMENT

This research was supported by the Israel Science Foundation, Minerva Stiftung, European Research Council (ERC) Advanced Grant (No. 338849), Helena and Martin Kimmel Center for Nanoscale Science, Moskowitz Center for Nano and Bio-Nano Imaging, and the Carolito Stiftung. E.J. holds the Drake Family Professorial Chair of Nanotechnology. SMS acknowledges funding from "Programa Internacional de Becas "la Caixa"-Severo Ochoa". JA and SMS acknowledge funding from Generalitat de Catalunya 2014 SGR 1638 and the Spanish MINECO project e-TNT (MAT2014-59961-C2-2-R). ICN2 acknowledges support from the Severo Ochoa Program (MINECO, Grant SEV-2013-0295). Part of the present work has been performed in the framework of Universitat Autònoma de Barcelona Materials Science PhD program. The HAADF-STEM microscopy was conducted in the Laboratorio de Microscopias Avanzadas at the Instituto de Nanociencia de Aragon-Universidad de Zaragoza. JA and SMS thank them for offering access to their instruments and expertise.

ABBREVIATIONS

VLS, vapor-liquid-solid; VS, vapor-solid; FIB, focused ion beam; HRTEM, high resolution transmission electron microscope; SEM, scanning electron microscope; AFM, atomic force microscope; PL, photoluminescence; NBE, near band-edge emission; DSE, defect state emission; EMCCD, electron multiplying charge-coupled device; TEM, transmission electron microscope; EDS, Energy-dispersive X-ray spectroscopy; HAADF, high angle angular dark-field; STEM, scanning transmission electron microscopy; GPA, geometric phase analysis.

REFERENCES

1. Dasgupta, N. P.; Sun, J.; Liu, C.; Brittman, S.; Andrews, S. C.; Lim, J.; Gao, H.; Yan, R.; Yang, P. 25th Anniversary Article: Semiconductor Nanowires – Synthesis, Characterization, and Applications. *Adv. Mater.* **2014**, *26*, 2137-2184.
2. Lu, W.; Lieber, C. M. Nanoelectronics from the Bottom Up. *Nat. Mater.* **2007**, *6*, 841-850.
3. Fan, Z.; Ho, J. C.; Jacobson, Z. A.; Yerushalmi, R.; Alley, R. L.; Razavi, H.; Javey, A. Wafer-Scale Assembly of Highly Ordered Semiconductor Nanowire Arrays by Contact Printing. *Nano Lett.* **2008**, *8*, 20-25.
4. Pan, C.; Dong, L.; Zhu, G.; Niu, S.; Yu, R.; Yang, Q.; Liu, Y.; Wang, Z. L. High-Resolution Electroluminescent Imaging of Pressure Distribution Using a Piezoelectric Nanowire LED Array. *Nat. Photonics.* **2013**, *7*, 752-758.
5. Huang, M. H.; Mao, S.; Feick, H.; Yan, H.; Wu, Y.; Kind, H.; Weber, E.; Russo, R.; Yang, P. Room-Temperature Ultraviolet Nanowire Nanolasers. *Science* **2001**, *292*, 1897-1899.
6. Yan, R.; Park, J.-H.; Choi, Y.; Heo, C.-J.; Yang, S.-M.; Lee, L. P.; Yang, P. Nanowire-Based Single-Cell Endoscopy. *Nat. Nanotechnol.* **2012**, *7*, 191-196.
7. Tian, B.; Zheng, X.; Kempa, T. J.; Fang, Y.; Yu, N.; Yu, G.; Huang, J.; Lieber, C. M. Coaxial Silicon Nanowires as Solar Cells and Nanoelectronic Power Sources. *Nature* **2007**, *449*, 885-889.

8. Wang, Z. L.; Song, J. Piezoelectric Nanogenerators Based on Zinc Oxide Nanowire Arrays. *Science* **2006**, *312*, 242-246.

9. Cui, Y.; Lauhon, L. J.; Gudiksen, M. S.; Wang, J.; Lieber, C. M. Diameter-Controlled Synthesis of Single-Crystal Silicon Nanowires. *Appl. Phys. Lett.* **2001**, *78*, 2214-2216.

10. Caroff,P.; Dick, K. A.; Johansson, J.; Messing, M. E.; Deppert, K.; Samuelson, L. Controlled Polytypic and Twin-Plane Superlattices in III-V Nanowires. *Nat. Nanotechnol.* **2009**, *4*, 50-55.

11. Pan, A.; Liu, R.; Sun, M.; Ning, C.-Z. Spatial Composition Grading of Quaternary ZnCdSSe Alloy Nanowires with Tunable Light Emission between 350 and 710 nm on a Single Substrate. *ACS Nano* **2010**, *4*, 671-680.

12. Gudiksen, M. S.; Lauhon, L. J.; Wang, J.; Smith, D. C.; Lieber, C. M. Growth of Nanowire Superlattice Structures for Nanoscale Photonics and Electronics. *Nature* **2002**, *415*, 617-620.

13. Trammell, T. E.; Zhang, X.; Li, Y.; Chen, L.-Q.; Dickey, E. C. Equilibrium Strain-Energy Analysis of Coherently Strained Core–Shell Nanowires. *J. Cryst. Growth* **2008**, *310*, 3084-3092.

14. Mårtensson, T.; Svensson, C. P. T.; Wacaser, B. A.; Larsson, M. W.; Seifert, W.; Deppert, K.; Gustafsson, A.; Wallenberg, L. R.; Samuelson, L. Epitaxial III−V Nanowires on Silicon. *Nano Lett.* **2004**, *4*, 1987-1990.

15. Yan, R.; Gargas, D.; Yang, P. Nanowire Photonics. *Nat. Photonics.* **2009**, *3*, 569-576.

16. Jiang, X.; Xiong, Q.; Nam, S.; Qian, F.; Li, Y.; Lieber, C. M. InAs/InP Radial Nanowire Heterostructures as High Electron Mobility Devices. *Nano Lett.* **2007**, *7*, 3214-3218.

17. Tomioka, K.; Motohisa, J.; Hara, S.; Hiruma, K.; Fukui, T. GaAs/AlGaAs Core Multishell Nanowire-Based Light-Emitting Diodes on Si. *Nano Lett.* **2010**, *10*, 1639-1644.

18. Qian, F.; Li, Y.; Gradecak, S.; Park, H.-G.; Dong, Y.; Ding, Y.; Wang, Z. L.; Lieber, C. M. Multi-Quantum-Well Nanowire Heterostructures for Wavelength-Controlled Lasers. *Nat. Mater.* **2008**, *7*, 701-706.

19. Heiss, M.; Fontana, Y.; Gustafsson, A.; Wüst, G.; Magen, C.; O'Regan, D. D.; Luo, J. W.; Ketterer, B.; Conesa-Boj, S.; Kuhlmann, A. V.; Houel, J.; Russo-Averchi, E.; Morante, J. R.; Cantoni, M.; Marzari, N.; Arbiol, J.; Zunger, A.; Warburton, R. J.;

Fontcuberta i Morral, A. Self-Assembled Quantum Dots in a Nanowire System for Quantum Photonics. *Nat. Mater.* **2013**, *12*, 439-444.

20. Wang, K.; Chen, J.; Zhou, W.; Zhang, Y.; Yan, Y.; Pern, J.; Mascarenhas, A. Direct Growth of Highly Mismatched Type II ZnO/ZnSe Core/Shell Nanowire Arrays on Transparent Conducting Oxide Substrates for Solar Cell Applications. *Adv. Mater.* **2008**, *20*, 3248-3253.
21. Wu, Z.; Zhang, Y.; Zheng, J.; Lin, X.; Chen, X.; Huang, B.; Wang, H.; Huang, K.; Li, S.; Kang, J. An All-Inorganic Type-IL Heterojunction Array with Nearly Full Solar Spectral Response Based on ZnO/ZnSe Core/Shell Nanowires. *J. Mater. Chem.* **2011**, *21*, 6020-6026.
22. Kempa, T. J.; Cahoon, J. F.; Kim, S.-K.; Day, R. W.; Bell, D. C.; Park, H.-G.; Lieber, C. M. Coaxial Multishell Nanowires with High-Quality Electronic Interfaces and Tunable Optical Cavities for Ultrathin Photovoltaics. *Proc. Natl. Acad. Sci. U. S. A.* **2012**, *109*, 1407-1412.
23. Storm, K.; Halvardsson, F.; Heurlin, M.; Lindgren, D.; Gustafsson, A.; Wu, P. M.; Monemar, B.; Samuelson, L. Spatially Resolved Hall Effect Measurement in a Single Semiconductor Nanowire. *Nat. Nanotechnol.* **2012**, *7*, 718-722.
24. van Weperen, I.; Plissard, S. R.; Bakkers, E. P. A. M.; Frolov, S. M.; Kouwenhoven, L. P. Quantized Conductance in an InSb Nanowire. *Nano Lett.* **2013**, *13*, 387-391.
25. Huang, Y.; Duan, X.; Wei, Q.; Lieber, C. M. Directed Assembly of One-Dimensional Nanostructures into Functional Networks. *Science* **2001**, *291*, 630-633.
26. Whang, D.; Jin, S.; Wu, Y.; Lieber, C. M. Large-Scale Hierarchical Organization of Nanowire Arrays for Integrated Nanosystems. *Nano Lett.* **2003**, *3*, 1255-1259.
27. Yao, J.; Yan, H.; Lieber, C. M. A Nanoscale Combing Technique for the Large-Scale Assembly of Highly Aligned Nanowires. *Nat. Nanotechnol.* **2013**, *8*, 329-335.
28. Tsivion, D.; Schvartzman, M.; Popovitz-Biro, R.; von Huth, P.; Joselevich, E. Guided Growth of Millimeter-Long Horizontal Nanowires with Controlled Orientations. *Science* **2011**, *333*, 1003-1007.
29. Tsivion, D.; Schvartzman, M.; Popovitz-Biro, R.; Joselevich, E. Guided Growth of Horizontal ZnO Nanowires with Controlled Orientations on Flat and Faceted Sapphire Surfaces. *ACS Nano* **2012**, *6*, 6433-6445.

30. Schvartzman, M.; Tsivion, D.; Mahalu, D.; Raslin, O.; Joselevich, E. Self-Integration of Nanowires into Circuits *Via* Guided Growth. *Proc. Natl. Acad. Sci. U. S. A.* **2013**, *110*, 15195-15200.

31. Nikoobakht, B.; Michaels, C. A.; Stranick, S. J.; Vaudin, M. D. Horizontal Growth and *in Situ* Assembly of Oriented Zinc Oxide Nanowires. *Appl. Phys. Lett.* **2004**, *85*, 3244-3246.

32. Hsin, C. L.; He, J. H.; Lee, C. Y.; Wu, W. W.; Yeh, P. H.; Chen, L. J.; Wang, Z. L. Lateral Self-Aligned P-Type In_2O_3 Nanowire Arrays Epitaxially Grown on Si Substrates. *Nano Lett.* **2007**, *7*, 1799-1803.

33. Fortuna, S. A.; Wen, J.; Chun, I. S.; Li, X. Planar GaAs Nanowires on GaAs (100) Substrates: Self-Aligned, Nearly Twin-Defect Free, and Transfer-Printable. *Nano Lett.* **2008**, *8*, 4421-4427.

34. Shen, Y.; Turner, S.; Yang, P.; Van Tendeloo, G.; Lebedev, O. I.; Wu, T. Epitaxy-Enabled Vapor–Liquid–Solid Growth of Tin-Doped Indium Oxide Nanowires with Controlled Orientations. *Nano Lett.* **2014**, *14*, 4342-4351.

35. Zi, Y.; Jung, K.; Zakharov, D.; Yang, C. Understanding Self-Aligned Planar Growth of InAs Nanowires. *Nano Lett.* **2013**, *13*, 2786-2791.

36. Yu, L.; Xu, M.; Xu, J.; Xue, Z.; Fan, Z.; Picardi, G.; Fortuna, F.; Wang, J.; Xu, J.; Shi, Y.; Chen, K.; Roca i Cabarrocas, P. In-Plane Epitaxial Growth of Silicon Nanowires and Junction Formation on Si(100) Substrates. *Nano Lett.* **2014**, *14*, 6469-6474.

37. Cheng, C.; Guo, H.; Amini, A.; Liu, K.; Fu, D.; Zou, J.; Song, H. Self-Assembly and Horizontal Orientation Growth of VO_2 Nanowires. *Sci. Rep.* **2014**, *4*, 5456-5460.

38. Nikoobakht, B.; Herzing, A. Where Is the Required Lattice Match in Horizontal Growth of Nanowires? *Nanoscale* **2014**, *6*, 12814-12821.

39. Wang, X.; Aroonyadet, N.; Zhang, Y.; Mecklenburg, M.; Fang, X.; Chen, H.; Goo, E.; Zhou, C. Aligned Epitaxial SnO_2 Nanowires on Sapphire: Growth and Device Applications. *Nano Lett.* **2014**, *14*, 3014-3022.

40. Oksenberg, E.; Popovitz-Biro, R.; Rechav, K.; Joselevich, E. Guided Growth of Horizontal ZnSe Nanowires and Their Integration into High-Performance Blue–UV Photodetectors. *Adv. Mater.* **2015**, *27*, 3999-4005.

41. Reut, G.; Oksenberg, E.; Popovitz-Biro, R.; Rechav, K.; Joselevich, E. Guided Growth of Horizontal P-Type ZnTe Nanowires. *J. Phys. Chem. C* **2016**, *120*, 17087-17100.

42. Du, W.; Yang, X.; Pan, H.; Ji, X.; Ji, H.; Luo, S.; Zhang, X.; Wang, Z.; Yang, T. Controlled-Direction Growth of Planar InAsSb Nanowires on Si Substrates without Foreign Catalysts. *Nano Lett.* **2016**, *16*, 877-882.

43. Wang, Q.; Li, J.; Lei, Y.; Wen, Y.; Wang, Z.; Zhan, X.; Wang, F.; Wang, F.; Huang, Y.; Xu, K.; He, J. Oriented Growth of $Pb_{1-X}Sn_xTe$ Nanowire Arrays for Integration of Flexible Infrared Detectors. *Adv. Mater.* **2016**, *28*, 3596-3601.

44. Shalev, E.; Oksenberg, E.; Rechav, K.; Popovitz-Biro, R.; Joselevich, E. Guided CdSe Nanowires Parallelly Integrated into Fast Visible-Range Photodetectors. *ACS Nano* **2017**, *11*, 213-220.

45. Goren-Ruck, L.; Tsivion, D.; Schvartzman, M.; Popovitz-Biro, R.; Joselevich, E. Guided Growth of Horizontal GaN Nanowires on Quartz and Their Transfer to Other Substrates. *ACS Nano* **2014**, *8*, 2838-2847.

46. Tsivion, D.; Joselevich, E. Guided Growth of Epitaxially Coherent GaN Nanowires on SiC. *Nano Lett.* **2013**, *13*, 5491-5496.

47. Tsivion, D.; Joselevich, E. Guided Growth of Horizontal GaN Nanowires on Spinel with Orientation-Controlled Morphologies. *J. Phys. Chem. C* **2014**, *118*, 19158-19164.

48. Choi, W.; Seabron, E.; Mohseni, P. K.; Kim, J. D.; Gokus, T.; Cernescu, A.; Pochet, P.; Johnson, H. T.; Wilson, W. L.; Li, X. Direct Electrical Probing of Periodic Modulation of Zinc-Dopant Distributions in Planar Gallium Arsenide Nanowires. *ACS Nano* **2017**, *11*, 1530-1539.

49. Jeon, H.; Ding, J.; Patterson, W.; Nurmikko, A. V.; Xie, W.; Grillo, D. C.; Kobayashi, M.; Gunshor, R. L. Blue-Green Injection Laser Diodes in (Zn,Cd)Se/ZnSe Quantum Wells. *Appl. Phys. Lett.* **1991**, *59*, 3619-3621.

50. Wu, Q.; Litz, M.; Zhang, X. C. Broadband Detection Capability of ZnTe Electro-Optic Field Detectors. *Appl. Phys. Lett.* **1996**, *68*, 2924-2926.

51. Peköz, R.; Raty, J. Y. Band Structure Modulation of ZnSe/ZnTe Nanowires under Strain. *Phys. Rev. B* **2011**, *84*, 165444-165451.

52. Bang, J.; Park, J.; Lee, J. H.; Won, N.; Nam, J.; Lim, J.; Chang, B. Y.; Lee, H. J.; Chon, B.; Shin, J.; Park, J. B.; Choi, J. H.; Cho, K.; Park, S. M.; Joo, T.; Kim, S. ZnTe/ZnSe (Core/Shell) Type-II Quantum Dots: Their Optical and Photovoltaic Properties. *Chem. Mater.* **2010**, *22*, 233-240.

53. Fujita, S.; Arai, S.; Itoh, K.; Moriai, F.; Sakaguchi, T. Green Electroluminescence in ZnSe–ZnTe Heterojunctions by Liquid-Phase Epitaxial Growth. *Appl. Phys. Lett.* **1972**, *20*, 317-318.

54. Peköz, R. *Ab Initio* Study of Structural and Electronic Properties of Single Crystal and Core/Shell II-VI Semiconductor Nanowires. *Comput. Mater. Sci.* **2016**, *123*, 158-163.

55. Seth, A. F.; Xiuling, L. Metal-Catalyzed Semiconductor Nanowires: A Review on the Control of Growth Directions. *Semicond. Sci. Technol.* **2010**, *25*, 024005-024025.

56. Du, D.; Srolovitz, D. J.; Coltrin, M. E.; Mitchell, C. C. Systematic Prediction of Kinetically Limited Crystal Growth Morphologies. *Phys. Rev. Lett.* **2005**, *95*, 155503-155506.

57. de la Mata, M.; Magen, C.; Gazquez, J.; Utama, M. I. B.; Heiss, M.; Lopatin, S.; Furtmayr, F.; Fernández-Rojas, C. J.; Peng, B.; Morante, J. R.; Rurali, R.; Eickhoff, M.; Fontcuberta i Morral, A.; Xiong, Q.; Arbiol, J. Polarity Assignment in ZnTe, GaAs, ZnO, and GaN-AlN Nanowires from Direct Dumbbell Analysis. *Nano Lett.* **2012**, *12*, 2579-2586.

58. Utama, M. I. B.; de la Mata, M.; Magen, C.; Arbiol, J.; Xiong, Q. Twinning-, Polytypism-, and Polarity-Induced Morphological Modulation in Nonplanar Nanostructures with Van Der Waals Epitaxy. *Adv. Funct. Mater.* **2013**, *23*, 1636-1646.

59. Day, R. W.; Mankin, M. N.; Gao, R.; No, Y.-S.; Kim, S.-K.; Bell, D. C.; Park, H.-G.; Lieber, C. M. Plateau–Rayleigh Crystal Growth of Periodic Shells on One-Dimensional Substrates. *Nat. Nanotechnol.* **2015**, *10*, 345-352.

60. Gabai, R.; Ismach, A.; Joselevich, E. Nanofacet Lithography: A New Bottom-up Approach to Nanopatterning and Nanofabrication by Soft Replication of Spontaneously Faceted Crystal Surfaces. *Adv. Mater.* **2007**, *19*, 1325-1330.

61. Schwarz, K. W.; Tersoff, J. Elementary Processes in Nanowire Growth. *Nano Lett.* **2011**, *11*, 316-320.

62. Cao, Y. Y.; Yang, G. W. Vertical or Horizontal: Understanding Nanowire Orientation and Growth from Substrates. *J. Phys. Chem. C* **2012**, *116*, 6233-6238.

63. Shen, Y.; Chen, R.; Yu, X.; Wang, Q.; Jungjohann, K. L.; Dayeh, S. A.; Wu, T. Gibbs–Thomson Effect in Planar Nanowires: Orientation and Doping Modulated Growth. *Nano Lett.* **2016**, *16*, 4158-4165.

64. Nikoobakht, B.; Herzing, A.; Muramoto, S.; Tersoff, J. Vapor–Liquid–Solid Etch of Semiconductor Surface Channels by Running Gold Nanodroplets. *Nano Lett.* **2015**, *15*, 8360-8364.

65. de la Mata, M.; Magén, C.; Caroff, P.; Arbiol, J. Atomic Scale Strain Relaxation in Axial Semiconductor III–V Nanowire Heterostructures. *Nano Lett.* **2014**, *14*, 6614-6620.

66. de la Mata, M.; Leturcq, R.; Plissard, S. R.; Rolland, C.; Magén, C.; Arbiol, J.; Caroff, P. Twin-Induced InSb Nanosails: A Convenient High Mobility Quantum System. *Nano Lett.* **2016**, *16*, 825-833.

67. Philipose, U.; Yang, S.; Xu, T.; Ruda, H. E. Origin of the Red Luminescence Band in Photoluminescence Spectra of ZnSe Nanowires. *Appl. Phys. Lett.* **2007**, *90*, 063103-063105.

68. Zhang, Y.; Wu, Z.; Zheng, J.; Lin, X.; Zhan, H.; Li, S.; Kang, J.; Bleuse, J.; Mariette, H. ZnO/ZnSe Type II Core–Shell Nanowire Array Solar Cell. *Sol. Energy Mater. Sol. Cells* **2012**, *102*, 15-18.

69. Shuvayev, V. A.; Kuskovsky, I. L.; Deych, L. I.; Gu, Y.; Gong, Y.; Neumark, G. F.; Tamargo, M. C.; Lisyansky, A. A. Dynamics of the Radiative Recombination in Cylindrical Nanostructures with Type-II Band Alignment. *Phys. Rev. B* **2009**, *79*, 115307-115315.

70. Yadav, S. K.; Sharma, V.; Ramprasad, R. Controlling Electronic Structure through Epitaxial Strain in ZnSe/ZnTe Nano-Heterostructures. *J. Appl. Phys.* **2015**, *118*, 015701-015704.

71. Zhang, X.; Pinion, C. W.; Christesen, J. D.; Flynn, C. J.; Celano, T. A.; Cahoon, J. F. Horizontal Silicon Nanowires with Radial p–n Junctions: A Platform for Unconventional Solar Cells. *J. Phys. Chem. Letters* **2013**, *4*, 2002-2009.

72. Hÿtch, M. J.; Snoeck, E.; Kilaas, R. Quantitative Measurement of Displacement and Strain Fields from Hrem Micrographs. *Ultramicroscopy* **1998**, *74*, 131-146.